Proceedings of the ASME 2013 Fluids Engineering Division Summer Meeting
FEDSM2013
July 7-11, 2013, Incline Village, Nevada, USA

FEDSM2013-16102

Study on Flow Characteristics Downstream of Annular Inlet Guide Vanes

Masanori Kudo
Graduate School of Mechanical Enginnering
Kogakuin University
Shinjuku, Tokyo, Japan

Koichi Nishibe
Faculty of Global Engineering
Kogakuin University
Shinjuku, Tokyo, Japan

Masayuki Takahashi
Graduate School of mechanical Engineering
Kogakuin University
Shinjuku, Tokyo, Japan

Kotaro Sato
Faculty of Global Engineering
Kogakuin University
Shinjuku, Tokyo, Japan

Yoshinobu Tsujimoto
Graduate School of Engineering Science
Osaka University
Osaka, Japan

ABSTRACT

The main objectives of the present study are to identify the dominant parameters responsible for the generation of unsteady flow, determine the conditions under which flow oscillations are produced and the relation between the flow characteristics and the number of vanes with identical solidity. The flow instabilities downstream of inlet guide vanes (IGV) are clarified experimentally and by numerical simulation. The conditions for the onset of flow instability, including the number of cells and the oscillation characteristics of the unsteady flow, are discussed based on measured pressure fluctuations and the propagating angular velocity ratio of the instability for various radius ratios (r_3/r_2). The effectiveness of adjusting the number of vanes to control the flow instabilities is also discussed.

INTRODUCTION

Variable inlet guide vanes (IGV), which are a type of swirling flow generator, are installed at the inlet of centrifugal compressors to reduce the inlet mach number of the rotor blades. Under lower flow rates, the vane angle (β_2) referring to Figure 1 is reduced to align the flow with the compressor blade motion. However, under such conditions, flow instabilities with specific frequency characteristics appear and the performance of the compressor is degraded [1-4]. In addition, the flow instabilities that occur downstream of the IGV have been shown to be different to the rotating stall of the blades, in that the flow oscillation amplitude is dependent on the number of cells and the chord length [4]. Similar flow instabilities can also occur in pump turbines. Recently, the relation between flow instabilities downstream of IGV and the S-shaped characteristics of pump turbine performance has been highlighted due to the increasing demand of pumped-storage hydroelectricity [5].

Experimental results have been reported for a swirl generator tested in a suction wind tunnel [1,2]. The fundamental frequency of velocity and pressure fluctuations were found to increase with the flow rate, although no effect of the blade span or chord length on the fundamental characteristics of the unsteady flow could be identified. Regardless, many details still remain to be explained, including the conditions for the onset of flow instability or the influence of the number of vanes on flow instability.

The present study involves an experiment and numerical simulations to clarify the mechanism of flow instabilities downstream of the IGV for various numbers of vanes under the condition of identical solidity. Typical flow patterns for various conditions (radius ratio r_3/r_2, vane angle β_2, number of vanes n) are demonstrated. The onset conditions, which include the number of cells and the unsteady flow characteristics for various cell numbers, are investigated based on measured pressure and velocity fluctuations. In addition, the effectiveness of adjusting the number of vanes is also discussed with respect to control of the turbulence intensity (RMS) of the flow instabilities, which are presented at the same exit flow angle ($\alpha 3$) and compared for various numbers of vanes with identical solidity.

NOMENCLATURE

C	:	Chord length [mm]
d	:	Diameter [mm]
h	:	Blade span [mm]
m	:	Number of cells
n	:	Number of blade
P	:	Pressure [Pa]

Q : Flow rate (two-dimensional) [m^2/s]
r : Radius [mm]
r_m : Radius of measurement point [mm]
s : Solidity
t : Time [s]
T : Cycle of flow instabilities [s]
u : Velocity in the x-direction [m/s]
$\bar{u}$: Time-averaged velocity in the x-direction [m/s]
u' : Fluctuation of velocity in the x-direction [m/s]
v : Velocity in the y-direction [m/s]
$\bar{v}$: Time-averaged velocity in the y-direction [m/s]
v' : Fluctuation of velocity in the y-direction [m/s]
V_r : Radial velocity [m/s]
V_θ : Circumferential velocity [m/s]
x,y : Coordinate axes as shown in Figure 1
α : Flow angle [deg]
β : Vane angle [deg]
ρ : Density [kg/m^3]

Subscripts

0 : Inlet of the device
1 : Leading edge of the vanes
2 : Trailing edge of the device
3 : Outlet of the device
m : Measurement
r : Radial direction
θ : Circumferential direction

EXPERIMENTAL APPARATUS AND METHOD

Figure 1(a) shows the coordinate system used for the IGV. The radii of the device inlet, the leading edge, the trailing edge, and the device outlet are denoted as r_0, r_1, r_2 and r_3, respectively. For simplification, the guide vanes are flat plates. A schematic diagram of the experimental apparatus is shown in Figure 1(b). The airflow is generated by a ring blower. The radial flow velocity between two parallel discs is calculated from the flow rate as measured using a variable area flow meter. Tangential velocity components are induced by guide vanes constructed of aluminum plates (chord: 20 mm, thickness: 1 mm and span: 10 mm). The vane angle β_2, measured from the tangential direction, can be changed arbitrarily. On the upper disc, the static pressure ports for measurement of the pressure fluctuations are connected to semiconductor pressure transducers (Toyota Koki PD104KW). The power spectrum and phase difference of the pressure fluctuations were analyzed using a fast Fourier transform (FFT) analyzer (Ono Sokki CF-5520) to determine the number of cells (see Ref. [3]). Various radius ratios (r_3/r_2=0.4, 0.5, 0.525, 0.55, 0.575, 0.6, 0.625, 065, 0.675, 0.7, 0.73) were achieved by exchanging the lower discs.

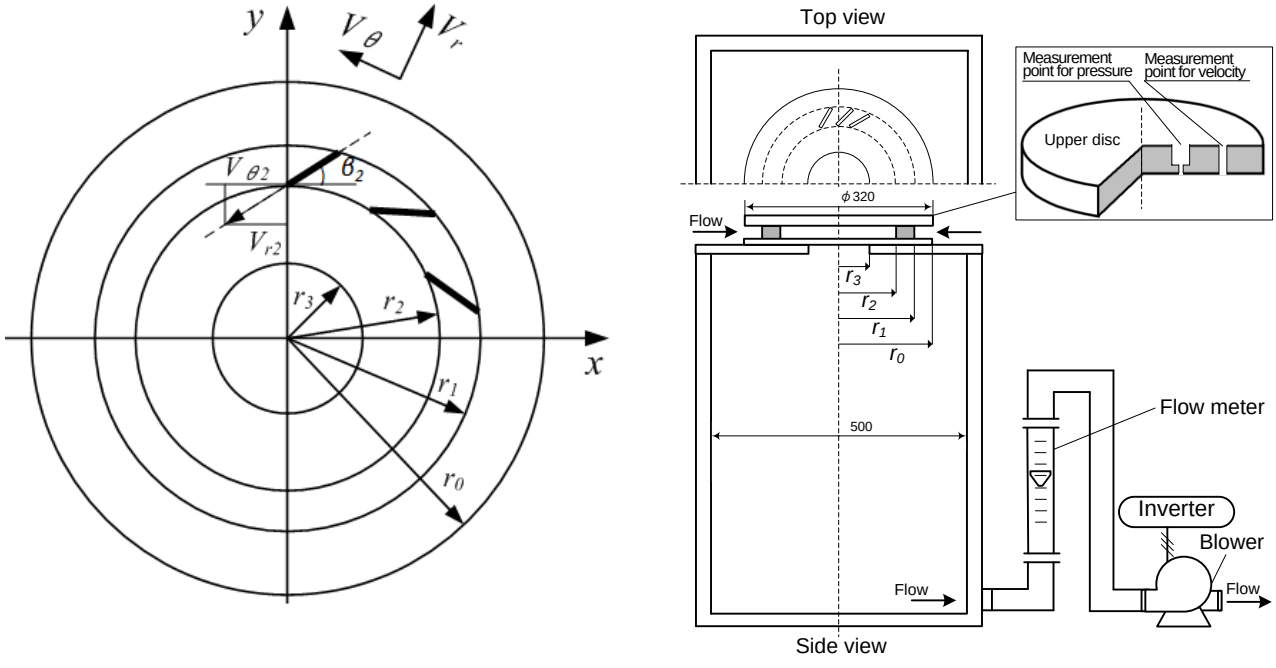

(a) Coordinate system **(b) Schematic diagram of the experimental apparatus**

Figure 1. Coordinate system and schematic diagram of the experimental apparatus

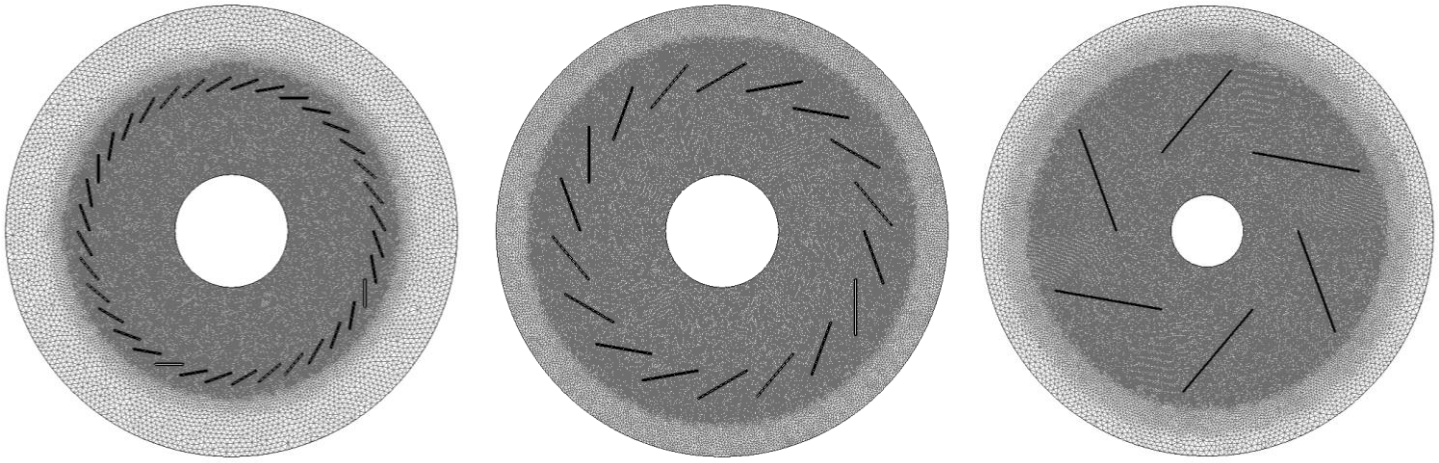

(a) n=36, C=20mm Number of mesh: 103378

(b) n=18, C=40mm Number of mesh: 105542

(c) n=6, C=120mm Number of mesh: 113280

Figure 2. Typical calculation mesh for various numbers of vanes and identical solidity (r_3/r_2=0.4, β_2=20deg, s=1.14)

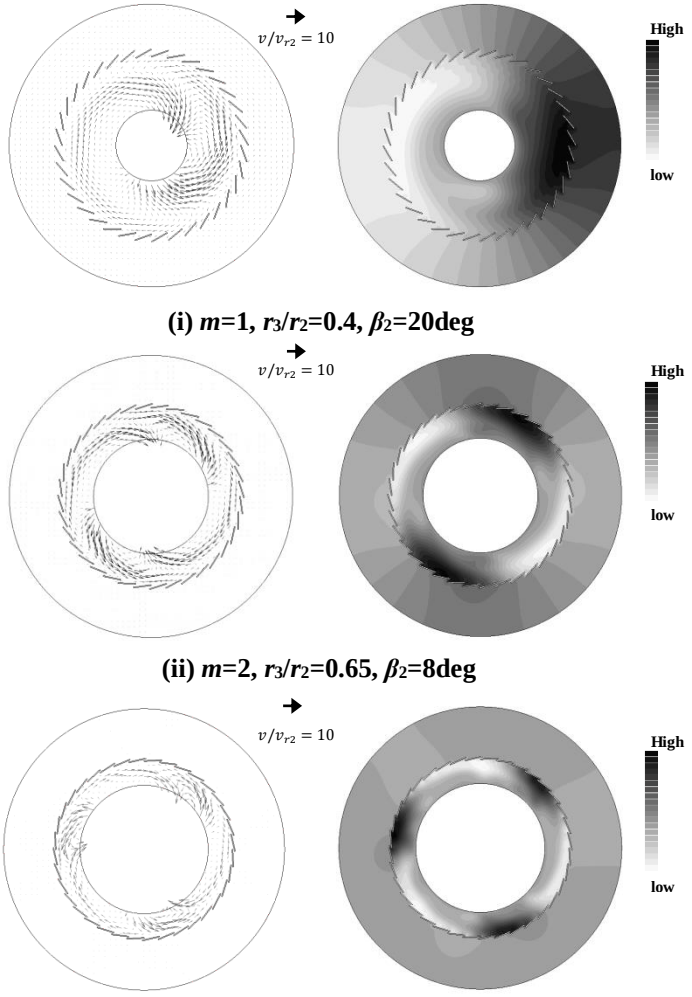

(i) m=1, r_3/r_2=0.4, β_2=20deg

(ii) m=2, r_3/r_2=0.65, β_2=8deg

(iii) m=3, r_3/r_2=0.73, β_2=3deg

(a) Velocity fluctuation **(b) Pressure fluctuation**

Figure 3. Distribution of velocity and pressure fluctuations ($n = 36, s = 1.14$)

NUMERICAL SIMULATION

Commercially available computer software was used to simulate two-dimensional laminar and incompressible flows in the computational fluid dynamics (CFD) simulation. The boundary conditions for constant radial flow velocity of the device inlet (r_0) and constant static pressure for the device outlet (r_3) were specified, in addition to the non-slip conditions at the vane surfaces and the slip conditions at the upper/lower disc surfaces. Figure 2 shows typical calculation meshes for the case with a radius ratio of r_3/r_2=0.4, a vane angle of β_2=20° and a solidity of s=1.14. Figures 2(a-c) show the cases for n=36 with C=20 mm, n=18 with C=40 mm, and n=6 with C=120 mm, respectively. The condition for identical solidity is fulfilled by decreasing the number of vanes and increasing the chord length. The solidity is defined as:

$$s=nCh/2\pi r_2 h \qquad (1)$$

RESULTS AND DISCUSSION

FUNDAMENTAL FLOW CHARACTERISTICS FOR 36 GUIDE VANES

In this report, only the results for s = 1.14 are discussed. Typical flow patterns for n=36 and C=20 mm obtained by numerical simulation are shown in Figure 3. Figure 3(a) shows vectors of velocity fluctuation and Fig. 3(b) shows the pressure fluctuation. In the case of r_3/r_2=0.4, β_2=20° (Figures 3(a, i) and (b, i)), a single cell (m=1) flow instability is observed. Figure 3(a, i) shows a velocity fluctuation that is periodically propagated in the circumferential direction per cycle and corresponds to a single cell. A pair of high-pressure (black) and low-pressure regions (white) is evident in Figure 3(b, i). Figures 3(a, ii) and 3(b, ii) (r_3/r_2=0.65, β_2=8°) show a velocity fluctuation that is periodically propagated in the circumferential direction per half cycle, and the two pairs of high-pressure (black) and low-pressure (white) regions correspond to two

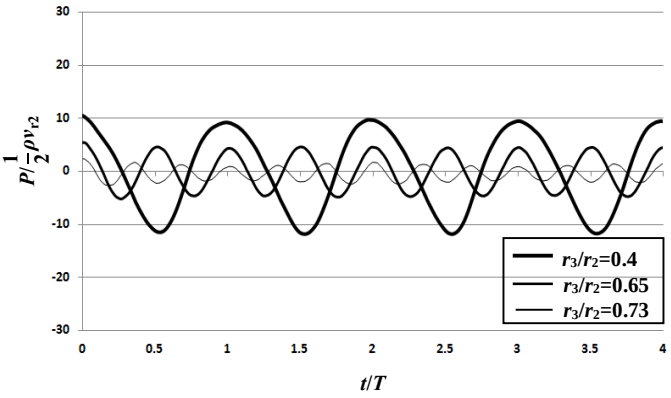

Figure 4. Influence of cell number on amplitude of pressure fluctuation measured experimentally (s=1.14, β_2=15 deg, C=20 mm)

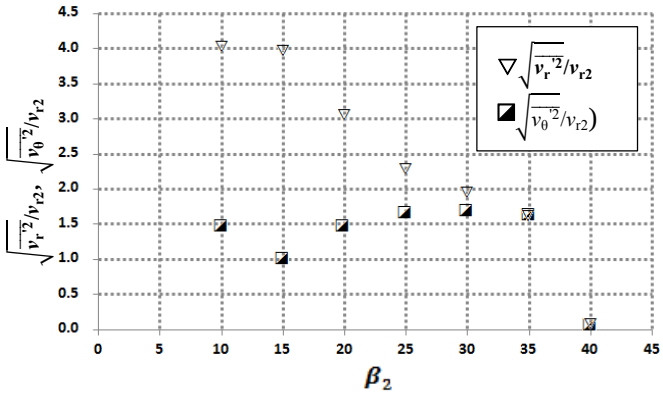

Figure 5. RMS on the outlet of the device in the case of constant 36 guide vanes (s=1.14, C=20mm, n=36, r_3/r_2=0.4)

cells (m=2). In addition, Figures 3(a, iii) and 3(b. iii) (r_3/r_2=0.73, β_2=3°) show a velocity fluctuation that is periodically propagated in the circumferential direction per one-third cycle, and the three pairs of high-pressure (black) and low-pressure (white) regions correspond to three cells (m=3). Therefore, it is concluded that the cell structure of flow instabilities downstream of annular IGV is significantly dependent on the radius ratio (r_3/r_2), the vane angle (β_2), and the number of vanes, where the vanes have identical solidity.

Figure 4 shows the pressure fluctuation with time at r_m/r_2 = 0.8 in the case of β_2=15° and C=20 mm. The horizontal axis represents non-dimensional time based on the cycle of flow instabilities (t/T) and the vertical axis represents the non-dimensional fluctuation of pressure ($p/0.5\rho v_{r2}^2$). Radius ratios of r_3/r_2=0.4, 0.65 and 0.73 correspond to a single cell, two cells and three cells, respectively. The non-dimensional amplitude of pressure fluctuation $p/0.5\rho v_{r2}^2$, is 10 for a single cell (m=1), 4 for double cells (m=2.5) and 1.0 for three cells (m=3). The amplitude of pressure fluctuation decreases as the numbers of cell increases.

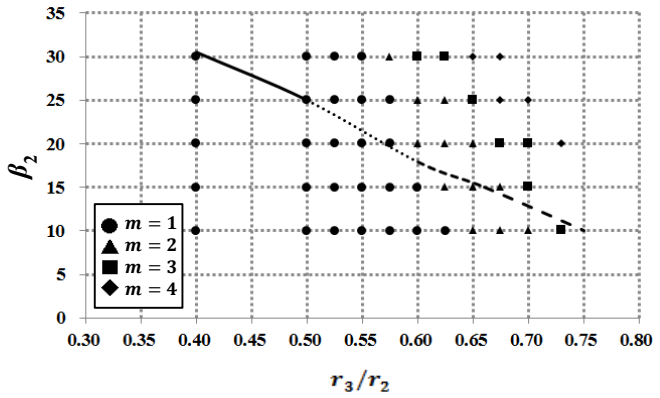

(a) Experimental

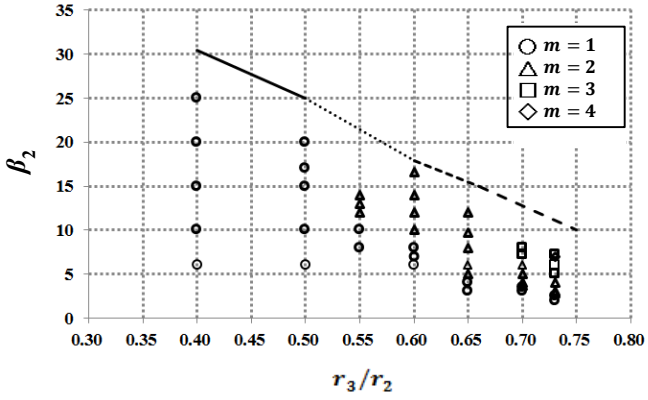

(b) CFD

Figure 6. Onset condition of the flow instabilities (C=20 mm, r_m/r_2=0.8)

1cell 2cells 3cells 4cells

Figure 5 shows the root mean square (*RMS*) of the velocity fluctuation at the device outlet in the case of n=36, C=20 mm and r_3/r_2=0.4, where the vertical axis represents the non-dimensional *RMS* of the radial velocity fluctuation and angular velocity fluctuations ($\sqrt{\overline{v_r'^2}}/v_{r2}$ and $\sqrt{\overline{v_\theta'^2}}/v_{r2}$). Note that both *RMS* values become larger than unity at β_2=35°, and then decrease to almost zero. The flow instabilities decrease as the vane angle β_2, increases.

For reasons of expediency, $\sqrt{\overline{v_r'^2}}/v_{r2} \geq 0.5$ is assumed as a condition for the generation of flow instabilities in this work.

The onset conditions, including the number of cells and the flow instabilities, are shown in Fig. 6 (onset condition map). Figures 6(a) and 6(b) show the experimental and numerical results, respectively. The horizontal axis represents the radius ratio (r_3/r_2), which corresponds to the circumferential velocity ratio ($V_{\theta 2}/V_{\theta 3}$). The analytical results from Ref. [3] are also shown (lines) for comparison. The experimental results, linear analysis and numerical simulation are in good qualitative

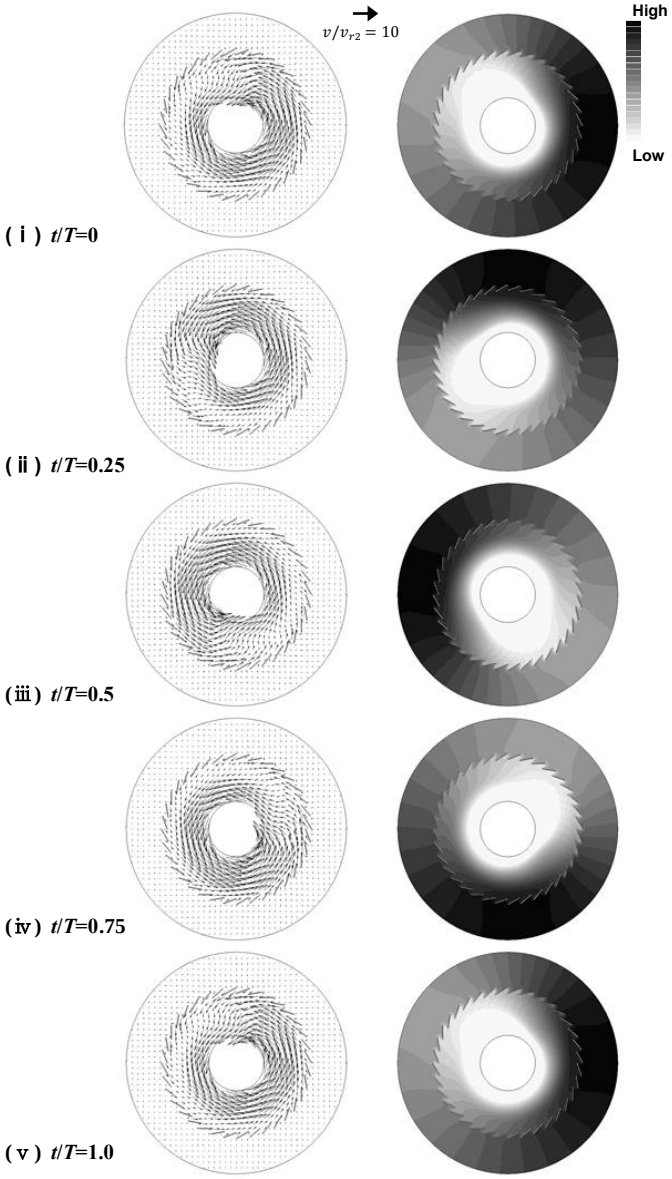

(a) Velocity vectors (b) Pressure distribution

Figure 7. Distribution of velocity vectors and pressure fluctuation by CFD (s=1.14, r_3/r_2=0.4, n=36, β_2=20 deg, α_3=15.0 deg)

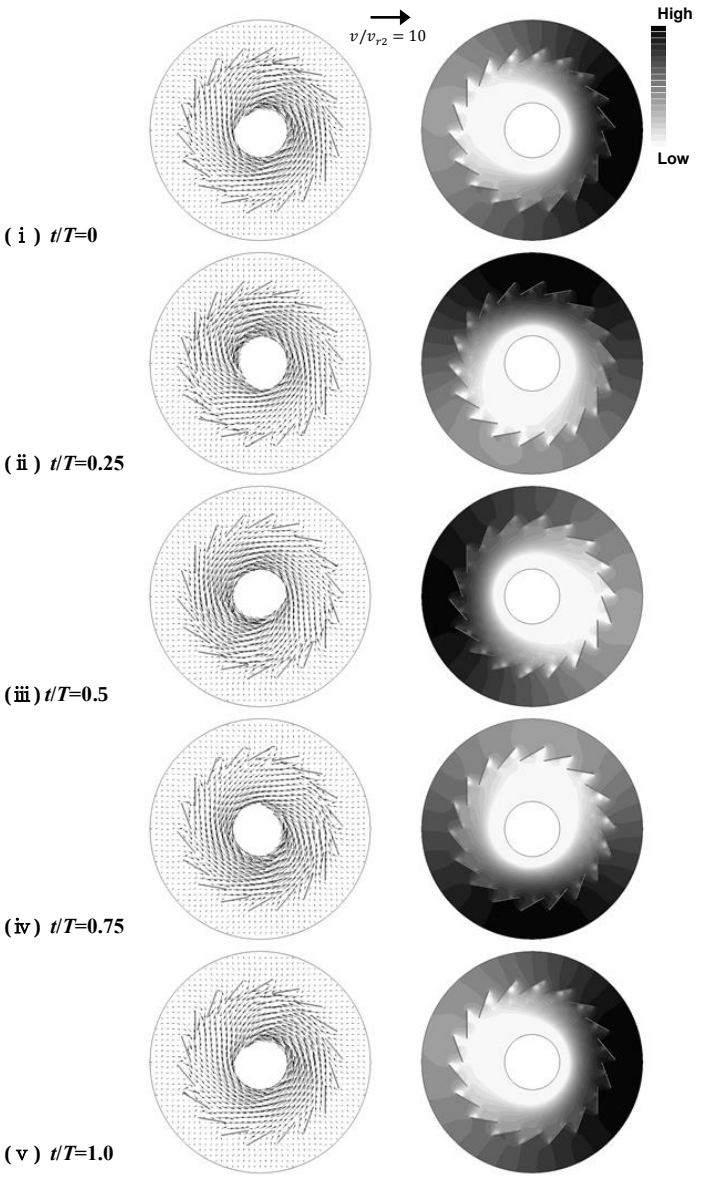

(a) Velocity vectors (b) Pressure distribution

Figure 8. Distribution of velocity vectors and pressure fluctuation by CFD (s=1.14, r_3/r_2=0.4, n=18, β_2=20 deg, α_3=20.2 deg)

agreement. The present investigation reveals that when the velocity gradient is large and the streamline is long, the number of cells is one. In addition, the number of cells in an unsteady flow is shown to be related to the circumferential velocity ratio and the vane angle. Smaller r_3/r_2 and β_2 result in more unstable flow, as shown in Figures 6(a) and 6(b). When the radius ratio r_3/r_2 is larger, multiple cells are generated with smaller fluctuation than that of a single cell. Smaller r_3/r_2 and β_2 result in higher amplitude and a longer cycle of flow instability is generated, as shown in Figures 6(a) and 6(b).

INFLUENCE OF THE NUMBER OF VANES ON THE FLOW INSTABILITIES

Figures 7, 8 and 9 show typical CFD results for various numbers of vanes and with r_3/r_2 = 0.4, β_2 = 20° and s = 1.14. The (a) and (b) figures show the velocity vector and pressure distributions, respectively. Panels (i) through (v) in Figures 7 and 8 show the distributions for t/T = 0, 0.25, 0.50, 0.75, and 1.0, respectively.

Figure 7 shows flow patterns for n=36, α_3 =15°, and C = 20 mm. Figure 7(a) shows regions of both positive and negative velocity fluctuations at the device exit (r=r_3), which indicates a

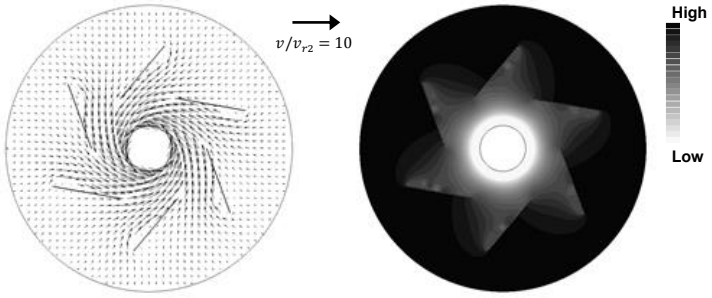

(a) Velocity vectors (b) Pressure distribution

Figure 9. Distribution of velocity vectors and pressure fluctuation by CFD (s=1.14, r_3/r_2=0.4, n=6, β_2=20 deg, α_3=32.8 deg)

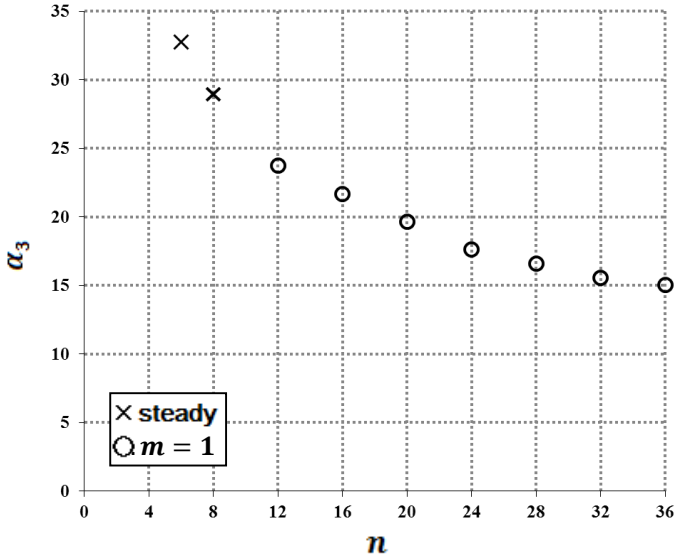

Figure 10. Influence of the number of vanes on flow angle α_3, for identical solidity (s=1.14,r_3/r_2=0.4, β_2=20 deg)

velocity distribution in the circumferential direction. In the present study, the pair of high-pressure (black) and low-pressure (white) regions that appears in Fig. 7(b) is defined as a single cell (m = 1). The flow instability is shown to rotate in an anti-clockwise direction.

Figure 8 shows flow patterns for n=18, α_3 =20.2°, and C =40 mm. The figures show no fundamental difference from the case presented in Figure 7. However, the reference vector is longer than that at n=36; therefore, the amplitude of the flow fluctuation is smaller than that for n=36.

Figure 9 shows flow fields for n=6, α_3 =32°, and C =120 mm. In this case, the flow becomes a steady flow without the formation of a cell structure.

Figure 10 shows the influence of the number of vanes on the exit flow angle α_3, for identical solidity. This numerical result was obtained for r_3/r_2=0.4 and β_2=20°. α_3 decreases with

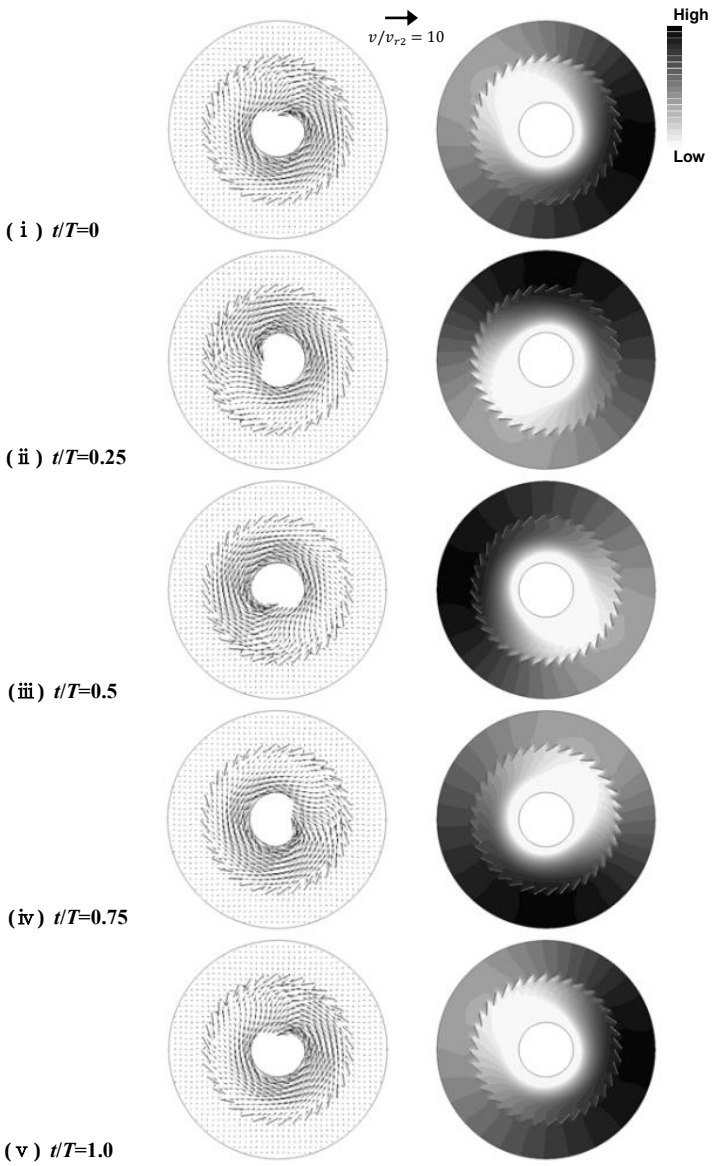

(a) Velocity vectors (b) Pressure distribution

Figure 11. Distribution of velocity vectors and pressure fluctuation by CFD (s=1.14, r_3/r_2=0.4, n=36, β_2=28 deg, α_3=20.3 deg)

increasing n; α_3 is dependent on n, even under the conditions of an identical vane angle β_2, and identical solidity, s. Furthermore, cell formation is not observed for n=6 and 8. However, the cause of stabilization could not be identified from Figures 9(a) and 9(b); whether the flow instabilities are controlled by reducing the number of vanes or by an increase in the exit flow angle.

Figures 11, 12 and 13 show the flow fields obtained by numerical calculation for various numbers of vanes and $\alpha_3 \cong$ 20°. The (a) and (b) figures show the distributions of the

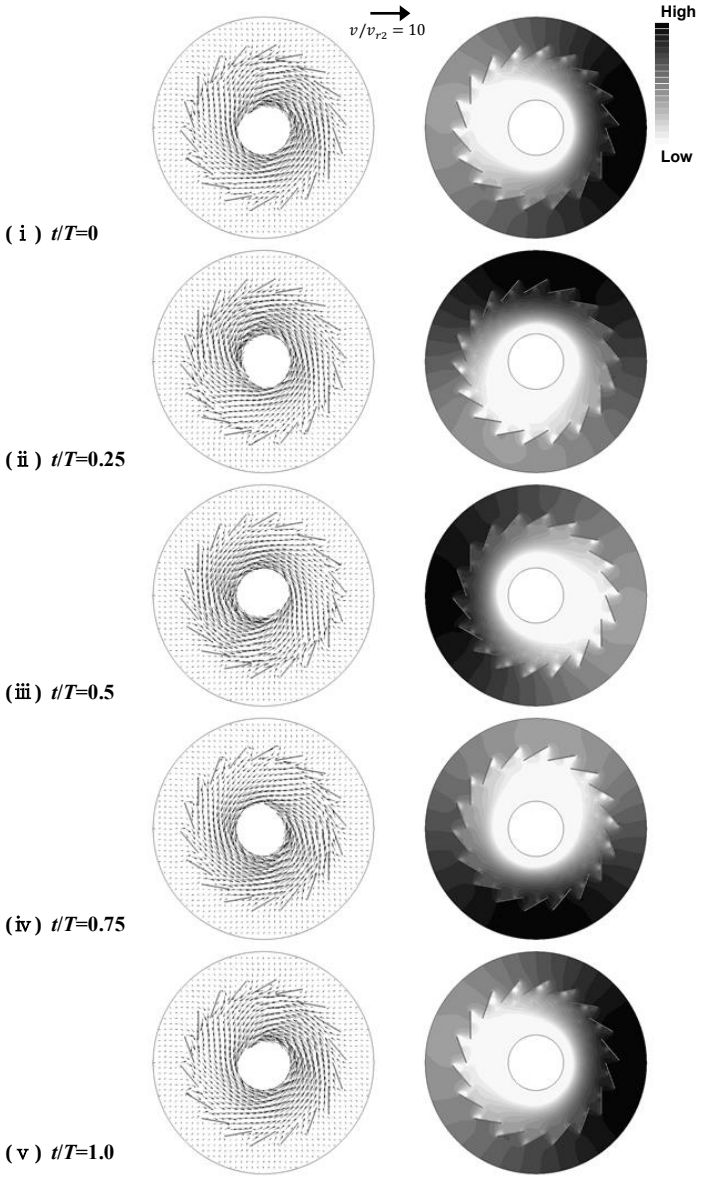

Figure 12. Distribution of velocity vectors and pressure fluctuation by CFD (s=1.14, r_3/r_2=0.4, n=18, β_2=20 deg, α_3=20.2 deg)

velocity vectors and pressure, respectively. In Figures 11 and 12, panels (i) through (v) show the distributions for t/T = 0, 0.25, 0.50, 0.75, and 1.0, respectively.

Under these conditions, the cell structures caused by flow instabilities propagate in an anti-clockwise direction, as shown in Figures 11 (n=36) and 12 (n=18). However, no circumferential velocity distribution is recognized in Figure 13 (n=6), although α_3 is the same at 20°. This indicates that when the number of vanes is small, the flow instability is suppressed, even with the same exit flow angle. For the case in which the

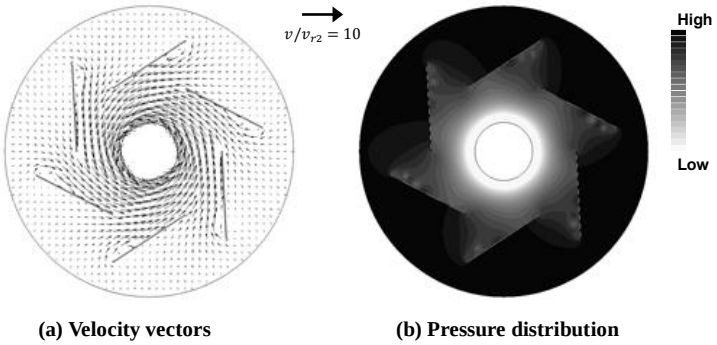

Figure 13. Distribution of velocity vectors and pressure fluctuation by CFD (s=1.14, r_3/r_2=0.4, n=6, β_2=3 deg, α_3=20.4 deg)

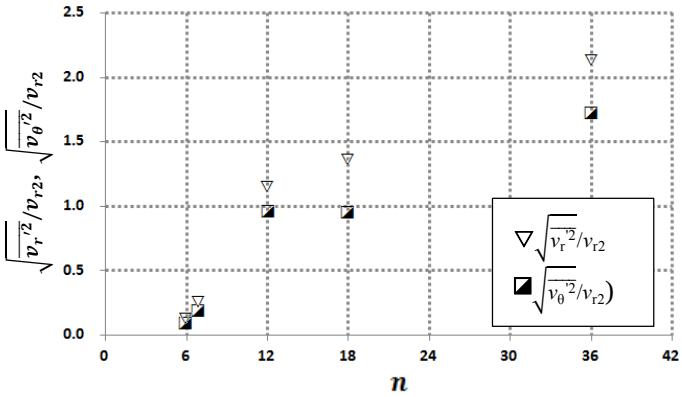

Figure 14. RMS for the device outlet with a constant exit flow angle (s=1.14, C=20 mm, α_3≈20 deg,r_3/r_2=0.4)

number of vanes is small, it is inferred that the generation of a cell structure is slowed down by the effect of the velocity distribution at the space between the vanes.

The influence of the number of vanes n, on the *RMS* ($\sqrt{\overline{v_r'^2}}/v_{r2}and\sqrt{\overline{v_\theta'^2}}/v_{r2}$) for r_3/r_2 =0.4 and α_3=20° is shown in Figure 14. The flow becomes almost steady flow for n=6 and 8, because the *RMS* becomes small with a decrease in the number of vanes. These results indicate the possibility of controlling flow instabilities by adjustment of the number of vanes.

CONCLUSION

An attempt was made to experimentally and numerically clarify the flow instabilities downstream of the IGV. The characteristics of flow instabilities and the conditions for the onset of flow instability were presented. Especially, the influence of the vane number on the flow instabilities was discussed. The findings obtained in this report are useful to replace the variable IGV to the annular circulation control wings. The circulation control wing that can adjust the flow

direction without change of geometry shape is adequate to produce swirling flow with flammable gas. Consequently, the following conclusions were arrived at:

(1) The amplitude of pressure fluctuation is dependent on the number of cells.
(2) The unsteady characteristics of flow instability were evaluated according to the RMS of velocity fluctuation.
(3) The onset condition can be identified in terms of the radius ratio and vane angle.
(4) The exit flow angle is not only dependent on the vane angle, but also on the number of vanes.
(5) The flow pattern of instability is dependent on the circumferential velocity distribution concerning to number of vanes.
(6) When the number of vanes is small, the flow instability is suppressed by the collapse of the circumferential dynamic balance, even with the same flow angle.

ACHNOWLEDGEMENTS

The present study was conducted with the support of a Grant-in-Aid for Scientific Research (21560187) and the Research Center for Urban Disaster Mitigation (UDM) of Kogakuin University.

REFERENCES

[1] Uchida, H., Bessho, A., Shiraki, M., Katagiri, H., Yagi,Y., and Takamura, T., 1994, "Development of Centrifugal Compressor for 100kw Automotive Ceramic Gas Turbine, Transactions of Gas Turbine Society of Japan", 21(84), pp.83-89.

[2] Takama, N. and Yoshiki, H., 1996, "Unstable Air Stream Arising near the Rear of Inlet Guide Vane, Effects of Guide Vane Width", Proceedings of the 11th Autumn Conference of Gas Turbine Society of Japan, 11, pp.19-22.

[3] Sato, K., Nagao, K., Tsujimoto, Y., Cho, K., and Yoshiki, H., 2000, "Study of Flow Instabilities Downstream of Radial Inlet Guide Vanes", Transactions of the Japan Society of Mechanical Engineers, 66(646), pp.1399-1406 .

[4] Koichi Nishibe, Kotaro Sato, Yoshinobu Tsujimoto and Haruo Yoshiki, 2011, "Control of Flow Instabilities Downstream of Radial Inlet Guide Vanes", Journal of Fluid Science and Technology Vol.6, No.4, pp.651-661.

[5] Vlad Hamatuchi, Mohamed Farhat, Steven Roth, Francisco Botero, Francois Avellan, 2011, "Experimental Evidence of Rotating Stall in a Pump-Turbine at Off-Design Condition in Generating Mode", Jorunal of Fluid Engineering, Vol.133.